Extraordinary magnetic response of an anisotropic 2D antiferromagnet via site-dilution

Junyi Yang[1], Hidemaro Suwa[2, *], Derek. Meyers[3,4], Han Zhang[1], Lukas Horak[5], Zhan Zhang[6], Evguenia Karapetrova[6], Jong-Woo Kim[6], Philip J. Ryan[6,7], Mark. P. M. Dean[3], Lin Hao[8,*] and Jian Liu[1, *]

[1]Department of Physics and Astronomy, University of Tennessee, Knoxville, Tennessee 37996, USA

[2]Department of Physics, University of Tokyo, Tokyo 113-8656, Japan

[3]Department of Condensed Matter Physics and Materials Science, Brookhaven National Laboratory, Upton, New York 11973, USA

[4]Department of Physics, Oklahoma State University, Stillwater, Oklahoma 74078, USA

[5]Department of Condensed Matter Physics, Charles University, Ke Karlovu 5, 12116 Prague, Czech Republic

[6]Advanced Photon Source, Argonne National Laboratory, Lemont, Illinois 60439, USA

[7]School of Physical Sciences, Dublin City University, Dublin 9, Ireland

[8]Anhui Key Laboratory of Condensed Matter Physics at Extreme Conditions, High Magnetic Field Laboratory, HFIPS, Chinese Academy of Sciences, Hefei, Anhui 230031, China

Sample synthesis and characterization

All SLs were prepared on (001)-oriented $SrTiO_3$ single crystal substrates by using a pulsed laser deposition system equipped with a reflection high-energy electron diffraction unit. All the substrates were pre-treated to have a uniform TiO_2 termination. During growth, the substrate temperature was fixed at 700 °C with pure oxygen pressure of 0.1 mbar. The laser fluency and frequency were optimized as 2 J/cm^2 and 10 Hz, respectively. A ceramic $SrIrO_3$ target and a single-crystal $SrTiO_3$ target were ablated alternately to realize the $[(SrIrO_3)_1/(SrTiO_3)_2]$ stacking sequence. The required pulse number of each $SrIrO_3$ layer was calculated using the corresponding growth rate of the pristine SL. The substitution was controlled by reducing the $SrIrO_3$ pulse number by δ followed by a subsequent deposition of $SrTiO_3$ until the entire layer is fully covered. The thicknesses of all the SLs were kept the same at 30 supercells. The structural properties of the SLs were first characterized by using a Panalytical X'Pert MRD diffractometer. Room-temperature synchrotron-based XRD measurements were performed on the 33BM beamline at Argonne National Laboratory with incident x-ray energy of 16 keV. The magnetic x-ray scattering measurements were performed on the 6IDB beamline at Argonne National Laboratory with incident x-ray energy around the Ir L_3-edge. A polarization analyzer was utilized to improve the signal-to-noise ratio of the magnetic peaks.

1) *c*-axis lattice parameter measurement

To determine the *c*-axis lattice parameter of the SLs, we measured (0 0 18) Bragg peaks of each SL at the 33BM beamline at Argonne National Laboratory. The peak position systematically increases with δ, confirming the shrinking *c*-axis lattice due to Ir^{4+} ions being substituted by the

smaller Ti^{4+} ions. The determined c-axis lattice parameters and extracted δ values from the expected lattice volume variation are listed in Table. S1.
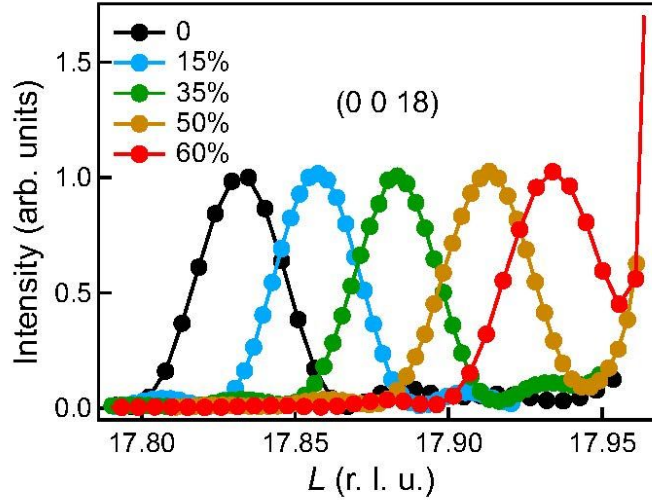

FIG. S1. Room-temperature L-scan across the (0 0 18) SL Bragg reflection measured along the substrate normal direction. Note that the reciprocal lattice here was defined as the $a \times a \times 3a$ superstructure cell, where a is the lattice parameter of the $SrTiO_3$ substrate.

Table. S1. c-axis lattice parameters and extracted δ values of the SLs.

Nominal δ	c-axis lattice parameter (Å)	Extracted δ
0	11.8263±0.00005	0
15%	11.8085±0.0003	16.0±0.5%
35%	11.7915±0.0001	31.3±0.2%
50%	11.7718±0.0004	49.0±0.6%
60%	11.7582±0.0004	61.2±0.7%

2) Epitaxial strain characterization

We have conducted reciprocal space mapping measurements on all the SLs. As shown in Fig. S2, for each SL, the in-plane lattice parameter is the same as that of the substrate. This demonstrates that all the SLs were coherently grown on the $SrTiO_3$ substrate and therefore have the same in-plane lattice parameter.
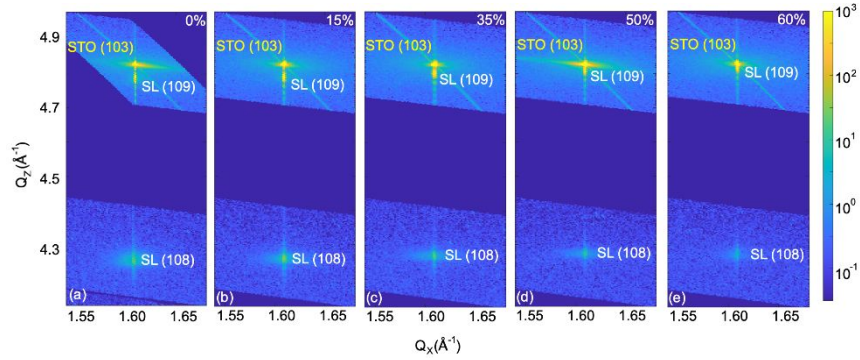

FIG. S2. Reciprocal space mapping measurements around the $SrTiO_3$ (103) Bragg reflection of SLs with $\delta = 0$ (a), 15% (b), 35% (c), 50% (d) and 60% (e).

3) Unveiling the "un*frustrated*" structure of the diluted superlattice

In the pristine SL, the giant AFM response roots in the U(1) symmetry of the $J_{eff} = 1/2$ pseudo-spins, which guarantees the exponential increase of AFM susceptibility while approaching the magnetic critical temperature, in combination with the effective staggered field effect [1]. The key of this effect is to preserve the spin continuous symmetry by fulfilling the so-called "*unfrustrated*" condition of the DM interactions [2], which requires the IrO_6 octahedra only rotate around the *c*-axis in a staggered manner within the square lattice. This distortion is dubbed as octahedral rotation, which can be characterized by measuring corresponding superstructure peaks,

like (0.5 1.5 3.5) in the pseudo-cubic notation [3, 4]. This symmetry could be broken by rotating the octahedron around the [110] axis, which is called octahedral tilting and can be checked by measuring superstructure peaks like (0.5 0.5 4.5) [4]. As shown in Fig. S3, clear superstructure peaks that indicates a pronounced octahedral rotation can be observed on each SL. As a comparison, we did not observe any octahedral tilting peaks within the experimental sensitivity. We thus demonstrate that all SLs meet the *"unfrustrated"* condition. With the crystal symmetry invariant against magnetic dilution, the diluted SLs retain the easy-plane anisotropy because of Hund's coupling [5].
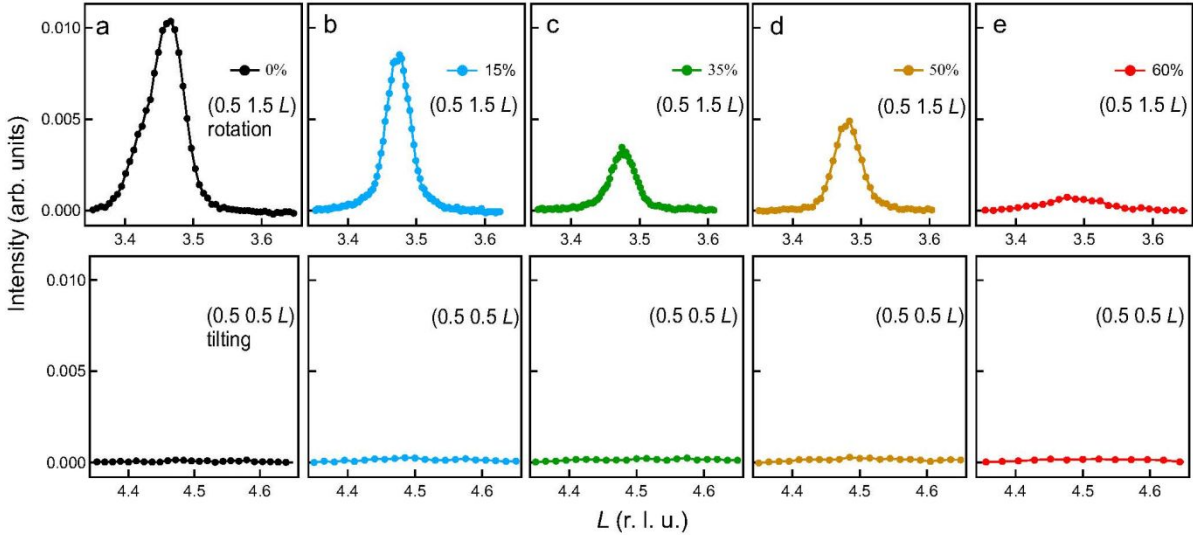

FIG. S3. Synchrotron-based XRD patterns across the octahedral rotation peak (0.5 1.5 3.5) on the SL with $\delta = 0$ (a), 15% (b), 35% (c), 50% (d) and 60% (e). The bottom panels list the octahedral tilting peak (0.5 0.5 4.5) for the corresponding SL.

4) Electrical transport properties measurements

The anisotropic Heisenberg Hamiltonian of the pseudospin-half moments assumes a Mott insulating ground state, which is often referred as the $J_{eff} = 1/2$ spin-orbital Mott insulator[6]. To

verify this state in our SLs, we measured DC resistivity on each SL using the standard four-point method. As shown in Fig. S4, the resistivity increases exponentially with decreasing temperature, unraveling a well-defined insulating ground state of each SL.
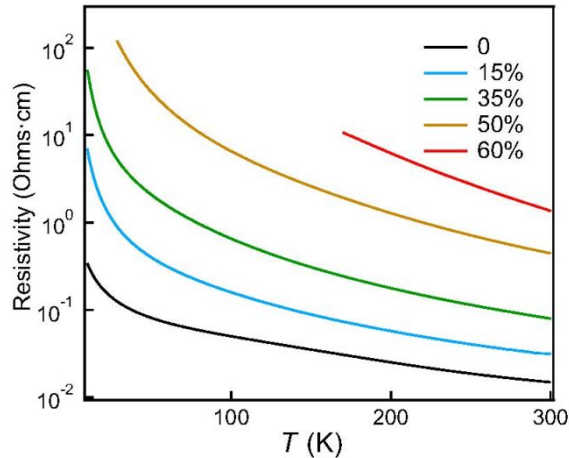

FIG. S4. DC resistivity as a function of temperature for the SLs. The resistivity of the SL with δ = 60% is out of the measurement limit below certain temperature.

Theoretical analysis and numerical methods

5) <u>General analysis on length scales introduced by perturbations to the 2D system</u>

As a representative case, let us consider the transition temperature of the quasi-2D Heisenberg model. Obtained from the random phase approximation [7, 8], the transition temperature introduced by an inter-plane coupling $J_\perp$ is given by the following scaling relation: $J_\perp \chi_{2D}(T_c) \sim 1$, where χ_{2D} is the susceptibility of the 2D Heisenberg model. This relation was confirmed by previous quantum Monte Carlo studies [9, 10]. Using the relation between the susceptibility and the correlation length ξ

in the 2D isotropic [11] (and also easy-plane anisotropic) case, $J\chi_{2D} \sim \xi^2$, where J is the in-plane energy scale, we obtain $J_\perp \xi^2(T_c) \sim J$. Thus, the inter-plane coupling introduces a length scale λ_{inter} $\sim \sqrt{J/J_\perp}$. The same argument can be applied to the (staggered) magnetic field perturbation. As a result, with h being the field strength, the external field introduces a length scale $\lambda_{\text{ext}} \sim \sqrt{J/h}$. Thus, when the correlation length reaches these length scales, the perturbation effects take place, introducing the transition or crossover temperatures.

6) <u>Quantum Monte Carlo simulation and fitting parameters</u>

The main interaction of the spin system is the intraplane isotropic Heisenberg interaction: $H_0 = \sum_{\langle i,j \rangle} \tilde{J}_{ij} \epsilon_i \epsilon_j \tilde{\mathbf{S}}_i \cdot \tilde{\mathbf{S}}_j$, where $\tilde{\mathbf{S}}_i$ is the pseudospin-half operator at site i in a rotating reference frame [1,5], ϵ_i takes 1 (0) with probability $1 - \delta$ (δ) independently for each site, and $\langle i,j \rangle$ runs over all the nearest and the next nearest neighboring pairs of each plane. The exchange couplings are $\tilde{J} \approx 600$ K and $\tilde{J}_2 \approx -\tilde{J}/4$, respectively. $\tilde{J} = \sqrt{J^2 + D^2}$ where $\frac{D}{J} = 0.27$ [1]. Here, the hidden SU(2) symmetry is restored by the staggered rotation by $\varphi \approx 10°$ around z axis perpendicular to the plane [5,12,13]. We need to take into account three kinds of perturbation to the main interaction. First, the small easy-plane anisotropy is introduced by the mixing of the $J_{\text{eff}} = 3/2$ orbitals [5], which is represented by $H_{\text{ani}} = -\tilde{J}\Gamma_1 \sum_{\langle i,j \rangle} \epsilon_i \epsilon_j \tilde{S}_i^z \tilde{S}_j^z$ with $\Gamma_1 \approx 10^{-4}$. Considering the anisotropy only of the nearest neighbor interaction suffices to capture the essence of physics. Secondly, a tiny interplane coupling remains in the SL [1]. The interplane exchange coupling is estimated to be $|J_\perp| \approx 0.006 \, \text{K}$ [1]. Thirdly, we control the AFM order by applying an in-plane magnetic field: $H_{\text{ext}} = -h\cos\varphi \sum_i \epsilon_i \tilde{S}_i^x + h\sin\varphi$

$\sum_i \epsilon_i e^{i\mathbf{Q}\cdot\mathbf{r}_i}\tilde{S}_i^y$, where $h = g_{aa}\mu_B B$ with the g-factor $g_{aa} \approx -2$ and the Bohr magneton μ_B, the

ordering vector $\mathbf{Q} = (\pi,\pi,\pi)$, and $\mathbf{r}_i$ is the coordinate of site i. Because of the staggered rotation of

the reference frame, the magnetic field couples linearly to the AFM order parameter [1].

We performed quantum Monte Carlo simulations for the 2D system described by $H_0 + H_{\text{ani}}$ up to

$2^{20}(\cong 10^6)$ spins, using the parallel loop algorithm [14, 15]. We obtained T_{BKT} and the parameter b

for each δ from the scaling of the transition temperature $T_{\text{BKT}}(L) = T_{\text{BKT}}(\infty)\left(1 + \frac{b^2}{4(\ln L)^2}\right)$ [16], where

L is the system length, and $T_{\text{BKT}}(L)$ is such that the Nelson-Kosterlitz relation

$\rho_s(T_{\text{BKT}}(L)) = \frac{2}{\pi}T_{\text{BKT}}(L)$ is satisfied. In the Monte Carlo simulation, we used periodic boundaries

and calculated the stiffness $\rho_s(T) = T[\langle W^2 \rangle]$, where W is the winding number of the worldline in

x (or y) direction, $\langle \cdot \rangle$ denotes the thermal average, and $[\cdot]$ denotes the random average. For each

δ, L, and T, the stiffness was averaged over more than 200 independent realizations of randomly

diluted spins.

We estimate $\frac{T_{\text{BKT}}}{J} \approx 0.213, 0.122,$ and 0.0339 for $\delta = 0, 15\%,$ and 35%, respectively, and $b \approx 3.4$

commonly. Fig. S5 clearly shows the data for $\delta = 0, 15\%,$ and 35% follow the asymptotic scaling

with the same value of b. For $L < \lambda_{\text{ani}} = 1/\sqrt{\Gamma_1}$, the system is ordered and the stiffness becomes

finite at the temperature such that the correlation length reaches the system size. The Nelson-

Kosterlitz relation is satisfied around this crossover temperature, which decreases with the system

size, as in the isotropic system. For $L \geq \lambda_{\text{ani}}$, the vortex starts forming when $\xi \approx \lambda_{\text{ani}}$. This

crossover temperature to the easy-plane ordered state does not depend much on L in the

intermediate system-size window $4\lambda_{\text{ani}} > L > \lambda_{\text{ani}}$, as shown in Fig. S5. For larger system sizes

$L \geq 4\lambda_{\text{ani}}$, the vortex pair forms a bonding state, and the T_{BKT} asymptotic scaling appears. The

observation of the same value of b is consistent with the vortex-bonding picture, in which the spin dilution is irrelevant to the critical theory of the pure 2D system. Fig. S5 also shows that the crossover length scale λ_{ani} does not depend much on δ, which is key to the length-scale switching. For $\delta = 50\%$, we calculated the stiffness at $T = 0$ without the anisotropy term H_{ani} and found ρ_s $(\delta = 50\%) \approx 0.02\rho_s(\delta = 0)$, which evidences that the case of $\delta = 50\%$ is not in the vortex-bonding regime but in the isotropic regime, as discussed in the main text. Using Eq. 2 from main text with $b \approx 3.4$ obtained from the Monte Carlo simulation, we fit the theoretical curve to the experimental data for $\delta = 0, 15\%$ and 35% simultaneously. We estimate $|J_{\perp}| \approx 0.006$ K and $c \approx 0.2$, which are consistent with the previous estimates [1].

It is noteworthy that it remains highly challenging to compute the crossover temperature of the $\delta = 50\%$ SL directly even with the-state-of-art method, due to the required heavy computation process and the infamous negative sign problem in the quantum Monte Carlo simulation [17]. Nevertheless, the exponential divergence of the correlation length $\xi \sim e^{\frac{2\pi\rho_s}{T}}$ in the renormalized classical regime is well established for the 2D isotropic Heisenberg model. This asymptotic form was confirmed by previous quantum Monte Carlo calculations with high precisions, such as the work in Ref. [18]. The scaling form of the crossover temperature (Eq. 3) deduced from the exponential divergence, was also confirmed by another quantum Monte Carlo calculation for magnetic anisotropy [19]. The same scaling form is naturally expected to be valid for other perturbations, such as (staggered) magnetic fields. Therefore, Eq. 3 with the optimal fitting parameters should produce the correct crossover temperature from the theoretical side. For $\delta = 50\%$, we use Eq. 3 and estimate $a \approx 0.1$ and $d \sim 10^{-6}$ K $\ll h$, which are reasonable.

7) <u>Scaling of the BKT transition</u>
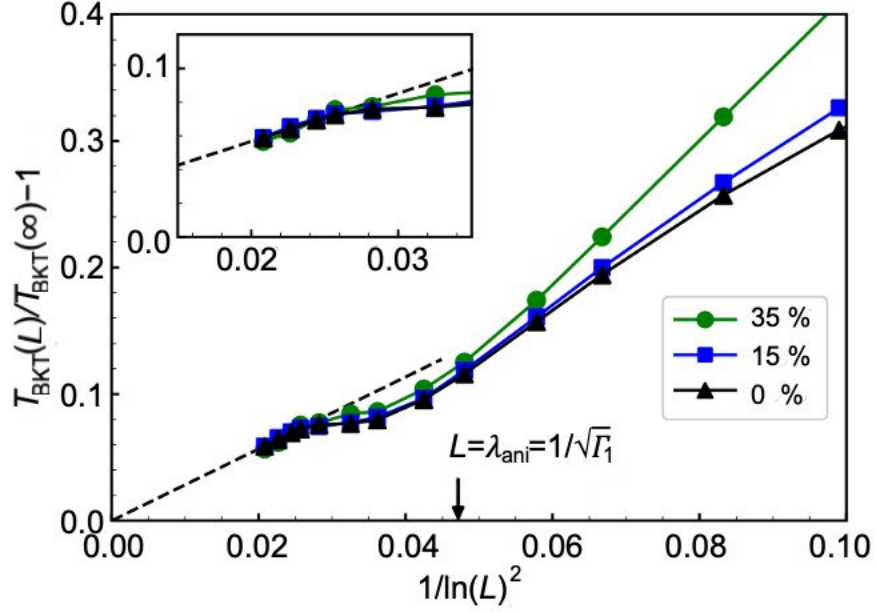

FIG. S5. Scaling of the BKT transition temperature that satisfies the Nelson-Kosterlitz relation $\rho_s(T_{\mathrm{BKT}}(L)) = \frac{2}{\pi}T_{\mathrm{BKT}}(L)$ obtained from quantum Monte Carlo simulations. The data for 0, 15, and 35% dilution show the asymptotic scaling with the same value of b and the crossover to the easy-plane state around the same length scale, $L = \lambda_{\mathrm{ani}} = 1/\sqrt{\Gamma_1}$.

8) <u>U(1) model in the vicinity of the percolation threshold</u>

To check whether or how the deviation of δ from nominal values would affect our main conclusion (especially for the δ=50% case), we calculated the crossover temperature for larger dilution fractions as a function of the external field. We here use the Nelson-Kosterlitz formula $\rho_s(T_{\mathrm{BKT}}) = \frac{2}{\pi}T_{\mathrm{BKT}}$ and a relation of the stiffness $\rho_s(0) \propto \rho_s(T_{\mathrm{BKT}})$ for the easy-plane spin system.

We then assume $T_{\text{BKT}}/\rho_s(0) \approx$ const., where the ratio depends on the easy-plane anisotropy but not on the dilution fraction for $\delta < \delta_p \approx 59.3\%$. We indeed confirmed the constant ratio for $\delta=0$, 15, 35, and 50% of the present 2D system. We also assume the scaling of the stiffness in the vicinity of the percolation threshold: $\rho_s(0) \propto (\delta_p - \delta)^t$, where $t \simeq 1.310$ is the conductivity exponent of the percolation transition. This scaling relation is obtained from the analogy to the random resistor network [20] and was tested for the isotropic SU(2) spin system [21]. This scaling form should hold even with a small easy-plane anisotropy and the next nearest neighbor interaction. We thus obtain the scaling of the BKT transition temperature $T_{\text{BKT}} \propto (\delta_p - \delta)^t$ for δ close to δ_p. Using the worldline quantum Monte Carlo method for the 2D system described by $H_0 + H_{\text{ani}}$, we calculated $\frac{T_{\text{BKT}}}{\tilde{J}} \approx 0.00467$ for $\delta=50\%$ and obtained the prefactor of the scaling. Using this scaling relation and Eq. (2), we calculated the crossover temperature curve for $\delta=55\%$, 56%, and 57%.
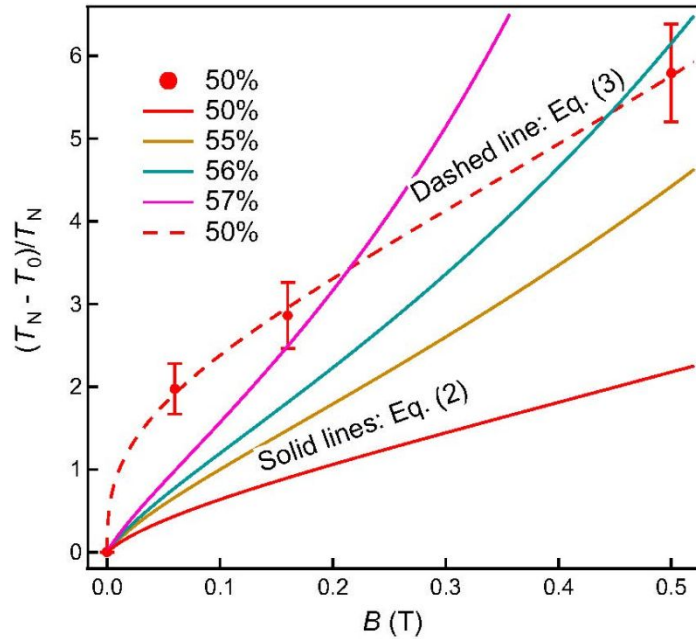
FIG. S6. Comparison between experimental data (red circles) and theoretical curves of the U(1) (solid line) and the SU(2) (dashed line) models for the δ=50% sample. Theoretical calculations of the U(1) model were performed also for δ=55%, 56% and 57%.

As shown in Fig. S6, the magnetic response is enhanced with increasing δ as expected. However, it is evident that the curve shape is substantially different from the experimental result: the curvature sign depends on the field strength, again pointing to the failure of the U(1) model in capturing the rapid increase of the crossover temperature. To produce the observed response at 0.5 T, δ must be as large as 56% in the U(1) model. Not only does this required value deviate too much from the extracted and the nominal values of δ, but also the responses at smaller fields are way too small compared with the experimental observation. This inconsistency with the experiment is fundamental to the U(1) model, indicating its limitation.

9) <u>Alternative analysis using the characteristic temperature of the inflection point</u>

To demonstrate the observed large magnetic response is intrinsic and does not depend on the definition of T_0, we also extracted the characteristic temperature of the inflection point for each SL under different magnetic fields. Note that, since the inflection point could not be reached for $\delta = 50\%$ due to the temperature limitation of the cryostat, we estimated its T_N as ~70% of the onset temperature according to the temperature dependence of other samples. As shown in Fig. S7, the systematic increase of magnetic response with δ and magnetic field well resembles the behavior of those defined with the onset temperature. More importantly, it is clear that the experimental data of the $\delta = 50\%$ sample is better described by the SU(2) model. We found that switching the definition of T_0 only resulted in a modification of the scaling prefactors, c in Eq.(2)

and a in Eq.(3), as expected. Given that T_N is estimated for $\delta = 50\%$, we also replaced T_N with the onset temperature in the normalization to obtain a lower bound of $(T_0 - T_N)/T_N$. Interestingly, even the lower bound is significantly larger than samples with smaller δ, further demonstrating the supremacy of the SU(2) model in explaining the experimental observation on the $\delta = 50\%$ sample.
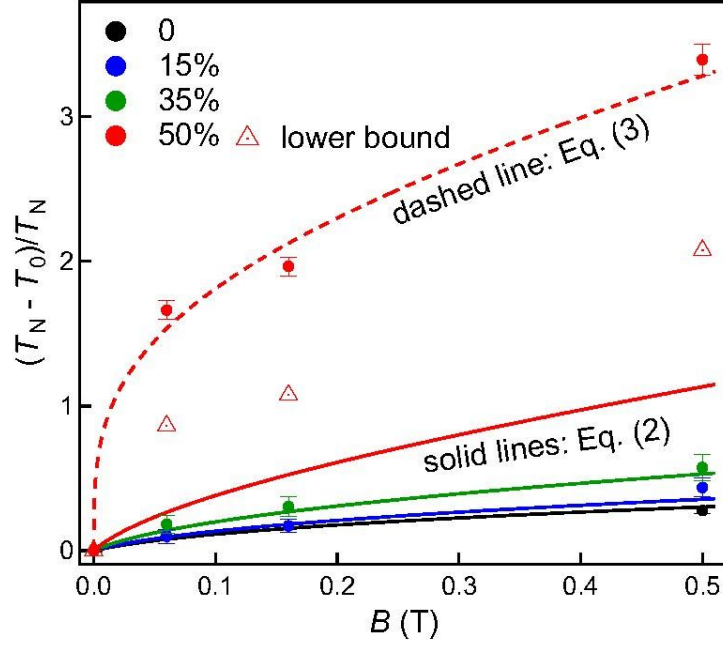

FIG. S7. $(T_0 - T_N)/T_N$ versus magnetic field (solid symbols). T_N and T_0 are characteristic temperatures of the inflection points at zero field and finite fields, respectively. Open triangles denote the lower bound of the $\delta = 50\%$ SL. Solid curves are theoretical analysis for $\delta = 0$ (black) , 15% (blue), 35% (green) and 50% (red) using Eq.(2). For $\delta = 50\%$, simulation using Eq.(3) is also shown (dashed).

References

1. Hao, L.; Meyers, D.; Suwa, H.; Yang, J.; Frederick, C.; Dasa, T. R.; Fabbris, G.; Horak, L.; Kriegner, D.; Choi, Y.; Kim, J.-W.; Haskel, D.; Ryan, P. J.; Xu, H.; Batista, C. D.; Dean, M. P. M.; Liu, J. Giant magnetic response of a two-dimensional antiferromagnet. *Nat. Phys.* **2018,** 14, 806–810.

2. Shekhtman, L.; Entin-Wohlman, O.; Aharony, A. Moriya's anisotropic superexchange interaction, frustration, and Dzyaloshinsky's weak ferromagnetism. *Phys. Rev. Lett.* **1992,** 69, (5), 836-839.

3. Glazer, A. M. The classification of tilted octahedra in perovskites. *Acta Cryst.* **1972,** B28, 3384-3392.

4. Glazer, A. M. Simple ways of determining perovskite structures. *Acta Cryst.* **1975,** A31, (6), 756-762.

5. Jackeli, G.; Khaliullin, G. Mott Insulators in the Strong Spin-Orbit Coupling Limit: From Heisenberg to a Quantum Compass and Kitaev Models. *Phys. Rev. Lett.* **2009,** 102, (1), 017205.

6. Kim, B. J.; Jin, H.; Moon, S. J.; Kim, J. Y.; Park, B. G.; Leem, C. S.; Yu, J.; Noh, T. W.; Kim, C.; Oh, S. J.; Park, J. H.; Durairaj, V.; Cao, G.; Rotenberg, E. Novel J_{eff}=1/2 Mott state induced by relativistic spin-orbit coupling in Sr_2IrO_4. *Phys. Rev. Lett.* **2008,** 101, (7), 076402.

7. Scalapino, D. J.; Imry, Y.; Pincus, P. Generalized Ginzburg-Landau theory of pseudo-one-dimensional systems. *Phys. Rev. B* **1975,** 11, (5), 2042-2048.

8. Schulz, H. J. Dynamics of Coupled Quantum Spin Chains. *Phys. Rev. Lett.* **1996,** 77, (13), 2790-2793.

9. Sengupta, P.; Sandvik, A. W.; Singh, R. R. P. Specific heat of quasi-two-dimensional antiferromagnetic Heisenberg models with varying interplanar couplings. *Phys. Rev. B* **2003,** 68, (9), 094423.

10. Yasuda, C.; Todo, S.; Hukushima, K.; Alet, F.; Keller, M.; Troyer, M.; Takayama, H. Neel Temperature of Quasi-Low-Dimensional Heisenberg Antiferromagnets. *Phys. Rev. Lett.* **2005,** 94, (21), 217201.

11. Chakravarty, S.; Halperin, B. I.; Nelson, D. R. Two-dimensional quantum Heisenberg antiferromagnet at low temperatures. *Phys. Rev. B* **1989,** 39, (4), 2344-2371.

12. Wang, F.; Senthil, T. Twisted Hubbard Model for Sr_2IrO_4: Magnetism and Possible High Temperature Superconductivity. *Phys. Rev. Lett.* **2011,** 106, (13), 136402.

13. Hao, L.; Wang, Z.; Yang, J.; Meyers, D.; Sanchez, J.; Fabbris, G.; Choi, Y.; Kim, J.-W.; Haskel, D.; Ryan, P. J.; Barros, K.; Chu, J.-H.; Dean, M. P. M.; Batista, C. D.; Liu, J. Anomalous magnetoresistance due to longitudinal spin fluctuations in a Jeff = 1/2 Mott semiconductor. *Nat. Commun.* **2019,** 10, (1), 5301.

14. Bauer, B.; Carr, L. D.; Evertz, H. G.; Feiguin, A.; Freire, J.; Fuchs, S.; Gamper, L.; Gukelberger, J.; Gull, E.; Guertler, S.; Hehn, A.; Igarashi, R.; Isakov, S. V.; Koop, D.; Ma, P. N.; Mates, P.; Matsuo, H.; Parcollet, O.; Pawłowski, G.; Picon, J. D.; Pollet, L.; Santos, E.; Scarola, V. W.; Schollwöck, U.; Silva, C.; Surer, B.; Todo, S.; Trebst, S.; Troyer, M.; Wall, M. L.; Werner, P.; Wessel, S. The ALPS project release 2.0: open source software for strongly correlated systems. *J. Stat. Mech.: Theo. Exp.* **2011,** 2011, (05), P05001.

15. Todo, S.; Matsuo, H.; Shitara, H. Parallel loop cluster quantum Monte Carlo simulation of quantum magnets based on global union-find graph algorithm. *Comput. Phys. Commun.* **2019,** 239, 84-93.

16. Bramwell, S. T.; Holdsworth, P. C. W. Magnetization and universal sub-critical behaviour in two-dimensional XY magnets. *J. Phys.: Condens. Matter* **1993,** 5, (4), L53-L59.

17. Troyer, M.; Wiese, U.-J. Computational Complexity and Fundamental Limitations to Fermionic Quantum Monte Carlo Simulations. *Phys. Rev. Lett.* **2005,** 94, (17), 170201.

18. Beard, B. B.; Birgeneau, R. J.; Greven, M.; Wiese, U. J. Square-Lattice Heisenberg Antiferromagnet at Very Large Correlation Lengths. *Phys. Rev. Lett.* **1998,** 80, (8), 1742-1745.

19. Cuccoli, A.; Roscilde, T.; Tognetti, V.; Vaia, R.; Verrucchi, P. Quantum Monte Carlo study of S= 1/2 weakly anisotropic antiferromagnets on the square lattice. *Phys. Rev. B* **2003,** 67, (10), 104414.

20. Grassberger, P. Conductivity exponent and backbone dimension in 2-d percolation. *Physica A* **1999,** 262, (3), 251-263.

21. Sandvik, A. W. Classical percolation transition in the diluted two-dimensional $S = 1/2$ Heisenberg antiferromagnet. *Phys. Rev. B* **2002,** 66, (2), 024418.